AUCTORES
Globalize your Research

Journal of Surgical Case Reports and Images

Vivien Hsu *

Open Access

Research Article

Theoretical investigation on Rh (III)-catalyzed cascade reaction of N-alkoxy carbamoyl indole with CF_3–ynone to synthesize pyrrolo[1,2-a] indole based on C–H activation

Nan Lu*, Chengxia Miao

College of Chemistry and Material Science, Shandong Agricultural University, Taian 271018, P. R. China

***Corresponding Author:** Nan Lu, College of Chemistry and Material Science, Shandong Agricultural University, Taian 271018, P. R. China.

Received Date: June 10, 2024; **Accepted Date:** June 17, 2024; **Published Date:** June 26, 2024

Citation: Nan Lu, Chengxia Miao, (2024), Theoretical investigation on Rh (III)-catalyzed cascade reaction of N-alkoxycarbamoyl indole with CF_3–ynone to synthesize pyr-rolo[1,2-a] indole based on C−H activation, *J, Surgical Case Reports and Images*, 7(5); **DOI:10.31579/2690-1897/198**

Abstract

The mechanism is investigated for Rh(III)-catalyzed cascade reaction of N-alkoxycarbamoyl indole with CF3–ynone and cascade transformation to cycloheptenone fused indole. The former contains cleavage of carbamoyl and indoyl bond giving five-membered rhodacycle via reversible CMD process, triple bond insertion into Rh−C after ynone coordination with Rh(III), proto-demetalation assisted by one HCl, extra MeOH embed into carbonyl determined to be rate-limiting, complex divided into indole and N-alkoxycarbamoyl unit, N-nucleophilic addition affording pyrrolo[1,2-a]indole and Rh(III) recover with second HCl. The latter is composed of rate-limiting Friedel−Crafts acylation initiated by ester cleavage forming MeOH and seven-membered cyclic ketone, the long range relay of H transfer arriving at α-C of indole, and β-elimination after dehydration. The positive solvation effect is suggested by decreased absolute and activation energies in solution compared with in gas. These results are supported by Multiwfn analysis on FMO composition of specific TSs, and MBO value of vital bonding, breaking.

Keywords: C-H activation; N-alkoxycarbamoyl; directing group; migratory insertion; rhodacycle

1 Introduction

Pyrrolo[1,2-a]indoles are privileged members pharmaceutically. As important natural products, they are also powerful molecules with antibacterial, antinociceptive, anti-inflammatory, and antitumor activities [1-3]. Among many representative examples, the derivatives with trifluoromethyl (CF_3) unit are especially sought-after in fields of biochemical, agrochemical, medicinal, and material sciences. Thus the synthesis of CF_3-pyrrolo[1,2-a]indole has received wide interest in recent years [4]. Many protocols could enable construction of carbon−carbon or carbon−heteroatom bond via photoredox, cascade, and transition-metal (TM)-catalyzed C−H bond activation (CHA) [5-7]. In this aspect, Yu developed the selective synthesis of dihydropyrimido[1,6-a]indol-1(2H)-ones via Rh(III)-catalyzed [3 + 3] or [4 + 2] C−H annulation [8]. Chen achieved Rh(III)-catalyzed selective olefination of N-carboxamide indoles with unactivated olefins via internal oxidation at room temperature [9]. Duan reported divergent synthesis of trifluoromethyl-substituted (dihydro)-pyrimidoindolones via Rh(III)-catalyzed C−H activation/annulation of N-carbamoylindoles with CF_3-imidoyl sulfoxonium ylides [10].

With wide application and rich reactivity in organic synthesis, CF_3-ynones were utilized creatively as coupling partners (CPs) for CHA reaction [11]. For example, 2,4-diaryl-6-trifluoromethylated pyridines was synthesized regioselectively through copper-catalyzed cyclization of CF_3-ynones and vinyl azides [12]. With anilines, 2-trifluoromethylquinolines was obtained through rhodium-catalysed redox-neutral [3 + 3] annulation [13]. Based on multiple bond activation, CF_3-tethered indazole derivatives was achieved via solvent-dependent selective synthesis [14]. Wang found cascade C(sp^2)−H and C(sp^3)−H bond cleavage in unusual reaction of 1-phenylpyrazolidinones toward diazonaphthalen-2(1H)-ones [15]. Shen got fluorinated pyridopyrimidinone in Rh(III)-catalyzed simultaneous [3 + 3]/[5 + 1] annulation of 1-arylpyrazolidinones with gem-difluorocyclopropenes [16]. Song applied unsymmetrical relay C−H alkenylation and [2 + 2] cycloaddition of N-arylsydnones with allenyl acetates to access quinoline-fused cyclobutanes [17]. There were also [4 + 1 + 1] annulation of N-aryl amidines with diazo homophthalimides and O_2, simultaneous indole construction and aryl introduction from 2-alkenylanilines and diazonaphthalen-2(1H)-ones and cascade reactions of N-nitrosoanilines with iodonium ylides leading to pyranone-tethered indazoles or carbazoles [18-20].

Since directing group (DG) is required to guarantee regioselectivity of

CHA reaction, N-alkoxylcarbamoyl indoles are important substrates containing easily removable or readily transformable DG [21]. Many advantages have been shown for Rh(III)-catalyzed oxidative [4+2] annulation of 2-arylquinoxalines, 2-aryl-2H-indazoles with allyl alcohols and switchable β-C(sp^2)–H alkenylation of acyclic enamides [22,23]. In this context, a breakthrough was Wang's [2 + 3] annulation of N-alkoxycarbamoyl indole with CF_3-ynone catalyzed by $[RhCp^*Cl_2]_2$ [24]. This novel method was also appliable to prepare cycloheptenone fused indole skeleton with remarkable biological activities [25]. Although this was the first example with N-alkoxycarbamoyl as effective DG for C2−H functionalization, many problems still puzzled and there was no report about detailed mechanistic study explaining the indispensable N-alkoxycarbamoyl group. Why the envisioned indole fused diazepine was not obtained and how unexpected pyrrolo-[1,2-a]indole product was yielded? What is the relation between C−H bond activation and N-alkoxycarbamoyl unit? How the acid-promoted cascade transformation gives cycloheptenone fused indole? To solve these questions in experiment, an in-depth theoretical study was necessary for this strategy leading to diverse functionalized pyrrolo[1,2-a]indole derivatives.

2 Computational details

The geometry optimizations were performed at the B3LYP/BSI level with the Gaussian 09 package [26,27]. The mixed basis set of LanL2DZ for Rh and 6-31G(d) for non-metal atoms [28-32] was denoted as BSI. Different singlet and multiplet states were clarified with B3LYP and ROB3LYP approaches including Becke's three-parameter hybrid functional combined with Lee−Yang−Parr correction for correlation [33-39]. The nature of each structure was verified by performing harmonic vibrational frequency calculations. Intrinsic reaction coordinate (IRC) calculations were examined to confirm the right connections among key transition-states and corresponding reactants and products. Harmonic frequency calculations were carried out at the B3LYP/BSI level to gain zero-point vibrational energy (ZPVE) and thermodynamic corrections at 353 K and 1 atm for each structure in methanol. The solvation-corrected free energies were obtained at the B3LYP/6-311++G(d,p) (LanL2DZ for Rh) level by using integral equation formalism polarizable continuum model (IEFPCM) in Truhlar's "density" solvation model [40-42] on the B3LYP/BSI-optimized geometries.

As an efficient method obtaining bond and lone pair of a molecule from modern ab initio wave functions, NBO procedure was performed with Natural bond orbital (NBO3.1) to characterize electronic properties and bonding orbital interactions [43,44]. The wave function analysis was provided using Multiwfn_3.7_dev package [45] including research on frontier molecular orbital (FMO) and Mayer bond order (MBO).

3 Results and Discussion

The mechanism was explored for (a) Rh(III)-catalyzed cascade reaction of N-alkoxycarbamoyl indole **1a** with CF_3–ynone **2** leading to pyrrolo[1,2-a]indole **3a** (b) cycloheptenone fused indole **4b** from pyrrolo[1,2-a]indole acetate **3b** (Scheme 1). Illustrated by black arrow of Scheme 2a, initially, Rh(III)-catalyzed carbamoyl N2-H bond and indoyl C1−H bond cleavage of **1a** gives five-membered rhodacycle **I** via two steps of reversible CMD process. After the removal of two HCl, the coordination of triple bond of **2** with Rh(III) of **I** furnishes intermediate **II**, from which the following migratory insertion of activated triple bond into Rh−C bond generates **III**. Next assisted by one additional HCl, proto-demetalation of **III** affords intermediate **IV**, which forms intermediate **i5** involving H-bond after the addition of an extra MeOH molecule to carbonyl group. Then, the N-alkoxycarbamoyl unit embeded in **i5** is removed to give **V** and **VI**. Subsequently, **V** undergoes concerted proton transfer and intramolecular N-nucleophilic addition to afford product **3a** (red arrow). Meanwhile with a second HCl, proto-demetalation of **VI** gives methyl methoxycarbamate (**VII**) and regenerates Rh(III) catalyst (blue arrow).

Displayed by black arrow of Scheme 2b, the cascade transformation is initiated by intramolecular Friedel−Crafts acylation of **3b** along with ester cleavage at 120 °C. The dissociated alkoxy group and hydrogen of benzene ring forming MeOH molecule leaves after the generation of seven-membered cyclic ketone **A**. Then, one hydrogen atom of methylene undergoes two times of proton migration arriving active α-C of indole, from which hydroxyl bonds with the eliminated β-H forming H_2O molecule to complete dehydration and the formation of desired product **4b**. The schematic structures of optimized TSs in Scheme 2 were listed by Figure 1. The activation energy was shown in Table 1 for all steps. Supplementary Table S1, Table S2 provided the relative energies of all stationary points. According to experiment, the Gibbs free energies in methanol solution phase are discussed here.

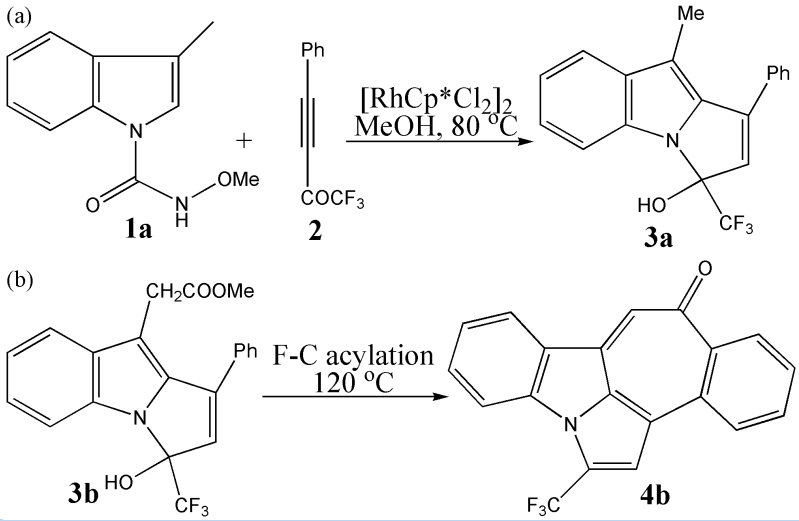

Scheme 1 (a) Rh(III)-catalyzed cascade reaction of N-alkoxycarbamoyl indole **1a** with CF_3–ynone **2** leading to pyrrolo[1,2-a]indole **3a** (b) cycloheptenone fused indole **4b** from pyrrolo[1,2-a]indole acetate **3b**.

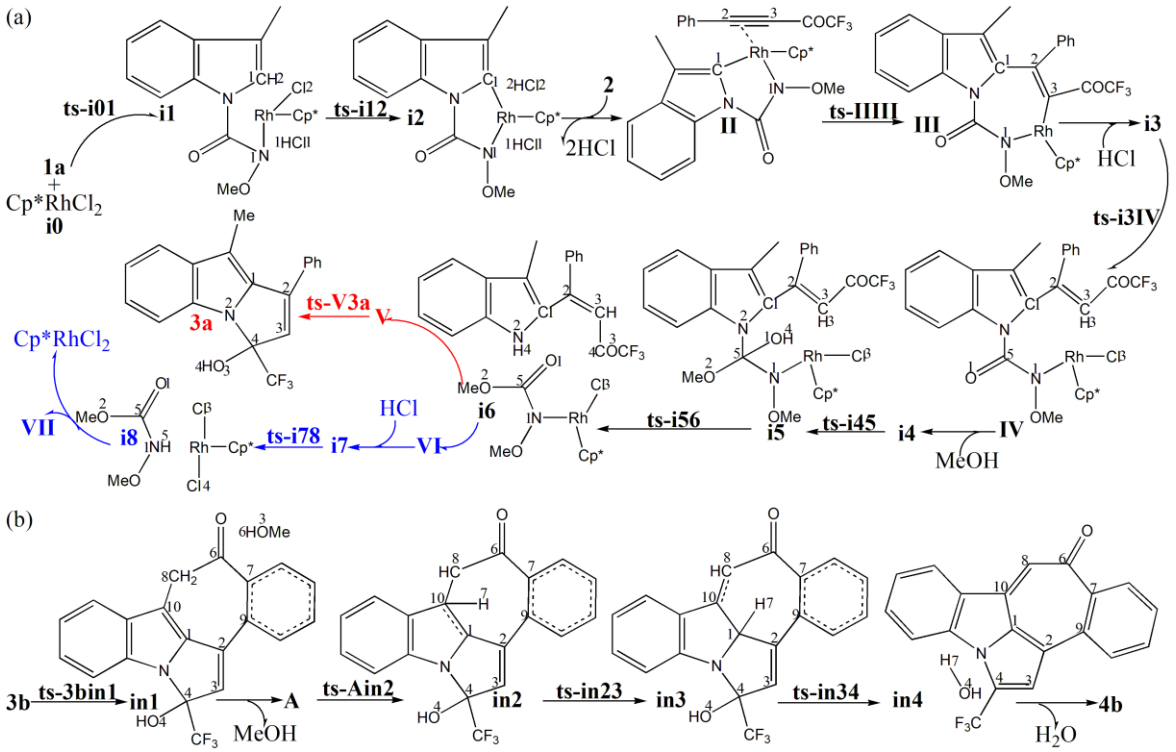

Scheme 2 Proposed reaction mechanism of (a) cascade reaction of **1a** with **2** leading to **3a** catalyzed by Cp^*RhCl_2 (b) **4b** from **3b**. TS is named according to the two intermediates it connects.

(a)

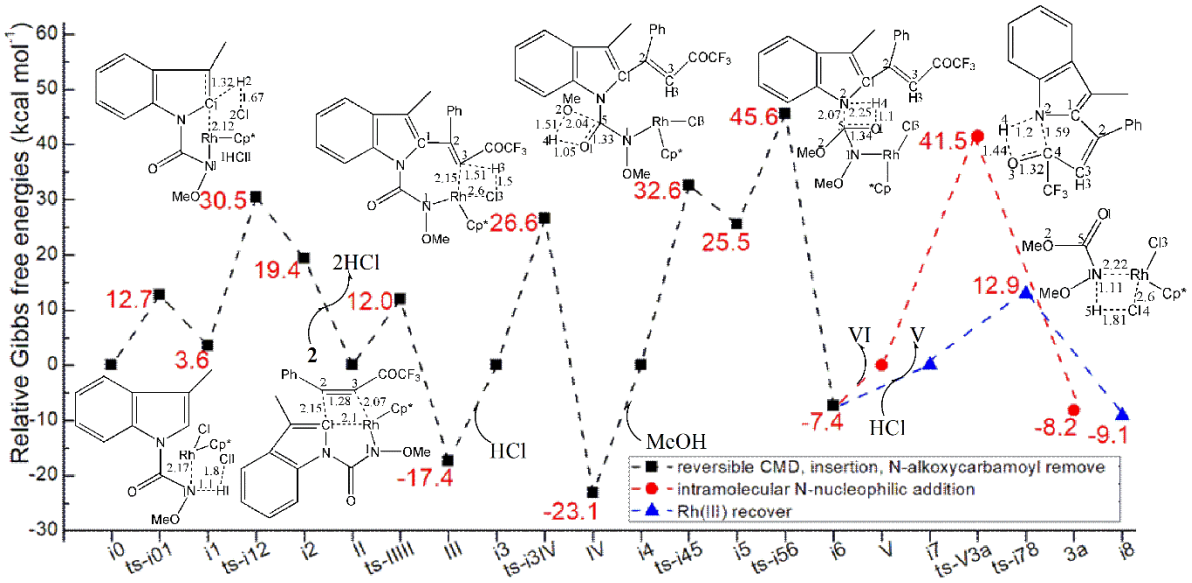

(b)

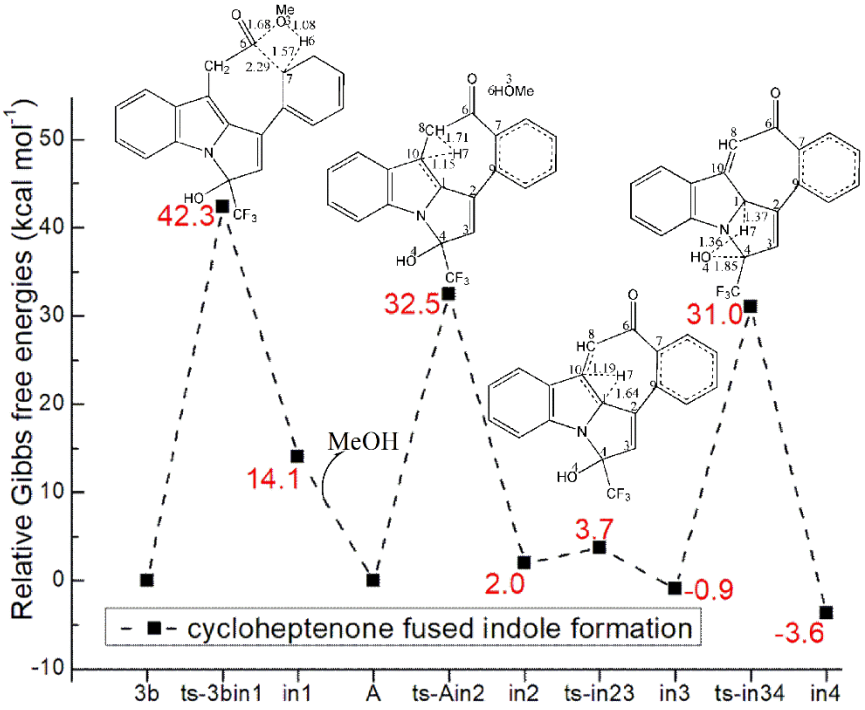

Figure 1. Relative Gibbs free energy profile in solvent phase starting from complex (a) **i0**, **II**, **i3**, **i4**, **V**, **i7** (b) **3b**, **A** (Bond lengths of optimized TSs in Å).

TS	$\Delta G^{\neq}_{gas}$	$\Delta G^{\neq}_{sol}$
ts-i01	21.3	12.7
ts-i12	22.4	26.9
ts-IIIII	14.5	12.0
ts-i3IV	23.0	26.6
ts-i45	33.8	32.6
ts-i56	19.6	20.1
ts-i78	16.1	12.9
ts-V3a	48.6	41.5
ts-3bin1	47.0	42.3
ts-Ain2	38.6	32.5
ts-in23	2.8	1.7
ts-in34	33.6	31.9

Table 1 The activation energy (in kcal mol^{-1}) of all reactions in gas and solvent

3.1 Reversible CMD process

Initially, the CMD process between **1a** and Cp^*RhCl_2 proceeds via **ts-i01** as step 1 with the activation energy of 12.7 kcal mol^{-1} relative to the starting point **i0** endothermic by 3.6 kcal mol^{-1} (black dash line of Figure 1a). Promoted by one Cl ligand of Rh(III) catalyst, the carbamoyl N1 is deprotonated as depicted by the transition vector including the transfer of H1 from N1 to Cl1 and coordination of Rh to N1 (1.1, 1.8, 2.17 Å). When H1-Cl1 is formed, Rh-N1 is also bonded in resultant intermediate **i1**.

From **i1**, the reactive indoyl α-C1 is deprotonated by another Cl ligand of Rh(III) catalyst forming a second H2-Cl2 molecule, which occurs via **ts-i12** with activation energy of 26.9 kcal mol^{-1} endothermic by 19.4 kcal mol^{-1} leading to **i2** in step 2. The transition vector contains concerted motion of C1⋯H2⋯Cl2 and cooperated Rh⋯C1 approaching (1.32, 1.67, 2.12 Å) (Figure S1a). The accomplish of Rh-C1 coordinated bond gives five-membered rhodacycle **I** along with two HCl in **i2**. Although barriers of this two steps are mediate at 80 °C in experiment, both endothermic indicates disfavorable process in thermodynamics, which echoes the prediction of reversible CMD by experiment.

3.2 Triple bond migratory insertion, proto-demetalation and methanol embed

After the removal of two HCl, an intermediate **II** is furnished via the coordination of ynone to Rh(III) and taken as new starting point for subsequent step 3. The migratory insertion of activated triple bond into Rh−C1 bond takes place via **ts-IIIII** with activation energy of 12.0 kcal mol^{-1} affording **III** exothermic by -17.4 kcal mol^{-1}. Clearly **III** is stable with the new seven-membered ring. The transition vector corresponds to the elongation of C2-C3 triple bond to double one, cleavage of Rh⋯C1 and simultaneous linkage of C1⋯C2, Rh⋯C3 (1.28, 2.10, 2.15, 2.07 Å) (Figure S1b).

The introduction of an additional HCl makes starting point denoted as **i3** for the following step 4 via **ts-i3IV** with a barrier of 26.6 kcal mol^{-1} exothermic by -23.1 kcal mol^{-1}delivering intermediate **IV**. Assisted by HCl, this proto-demetalation includes protonation and ring opening at C3. That is H3⋯C3 bonding and Rh⋯C3 breaking suggested by the transition vector, which also contains the afore required departure of Cl3-H3 and the after formation of Rh-Cl3 (1.51, 2.15, 1.50, 2.60 Å) (Figure S1c). The heat release of this two steps effectively pulls the entire reaction process thermodynamically.

From **IV**, the addition of an extra MeOH generates **i4** as starting point of next step 5. The MeOH is divided into alkoxy MeO and proton H two parts and inserted to C5-O1 carbonyl group. This step proceeds via **ts-i45** with activation energy of 32.6 kcal mol^{-1} endothermic by 25.5 kcal mol^{-1} yielding reactive intermediate **i5**. The transition vector is composed of remarkable O2⋯H4 fracture, extension of C5-O1 bond from double to single and bonding of C5⋯O2, O1⋯H4 (1.51, 1.33, 2.04, 1.05 Å) (Figure S1d). Here **i5** is active involving the embedded N-alkoxycarbamoyl unit and O1-H4⋯N2 H-bond ready for the following split into two parts.

3.3 N-alkoxycarbamoyl unit remove, intramolecular N-nucleophilic addition and Rh(III) recover

Then **i5** is removed into indole and N-alkoxycarbamoyl unit two parts denoted as **V** and **VI** respectively. The step 6 takes place via **ts-i56** with activation energy of 20.1 kcal mol^{-1} forming stable **i6** exothermic by -7.4 kcal mol^{-1}. According to the transition vector, the atomic motion predicts asynchronous complicated process of the prior N2⋯C5 dissociation, laggered O1⋯H4⋯N2 proton giving and the resulting C5⋯O1 shortened from single to double (2.07, 1.10, 2.25, 1.34 Å) (Figure S1e). Since this step is key to the product generation and catalyst recover simultaneously, the low barrier and heat release confirms the advantage from both kinetics and thermodynamics, which verifies the efficiency of this novel reaction pattern theoretically.

Subsequently via **ts-V3a**, **V** undergoes intramolecular N-nucleophilic addition followed by concerted proton transfer producing **3a** (red dash line of Figure 1a). The activation energy of step 7 is 41.5 kcal mol^{-1} relative to **V** exothermic by -8.2 kcal mol^{-1}. Without Rh(III) catalyst, this barrier becomes somewhat high yet capable to overcome under 80 °C in experiment. The detailed motion can be demonstrated by the transition vector (Figure S1f). That is N-nucleophilic attack of N2 to C4, proton H4 transferring from N2 to O3 and subsequent stretching of C4-O3 from double to single (1.59, 1.20, 1.44, 1.32 Å). The functionalized pyrrolo[1,2-a]indole is achieved as the ring closing of five-membered pyrrole.

Meanwhile a second H5-Cl4 is required for Rh(III) catalyst regeneration in step 8 via **ts-i78** with activation energy of 12.9 kcal mol^{-1} exothermic by -9.1 kcal mol^{-1} generating **i8** binding RhCp*Cl_2 and **VII** (blue dash line of Figure 1a). The transition vector of this second protodemetalation is about coordination shift from of N1⋯Rh to Rh⋯Cl4 and proton H5 given by Cl4 to N1 (2.22, 2.60, 1.81, 1.11 Å).

Under the promotion of Rh(III), the MeOH embed into carbonyl group via **ts-i45** is determined to be rate-limiting. This clarifies why N-alkoxycarbamoyl group is indispensable for C−H bond activation in experiment. Furthermore, the product generation and catalyst recover are both favorable thermodynamically. To highlight the idea of feasibility for changes in electron density and not molecular orbital interactions are responsible of the reactivity of organic molecules, quantum chemical tool Multiwfn was applied to analyze of electron density such as MBO results of bonding atoms and contribution of atomic orbital to HOMO of typical TSs (Table S3, Figure S2). These results all confirm the above analysis.

3.4 Cycloheptenone fused indole formation

In view of another product **4b** attractive biologically, the cascade transformation from **3b** is also explored as is displayed by black arrow of Scheme 2b. Without the effective Rh(III), the whole process demands higher 120 °C especially the initial intramolecular Friedel−Crafts acylation via **ts-3bin1**. The activation energy of step 1 is 42.3 kcal mol^{-1} relative to the starting point **3b** endothermic by 14.1 kcal mol^{-1} (black dash line of Figure 1b). As acyl donor, the ester bond C6⋯O3 breaks and the bonding C6⋯C7 replaces H6 on benzene ring. The dissociated alkoxy MeO3 group combines with H6 and leaves as a methanol MeOH molecule. This can be illustrated in detail by the transition vector (1.68, 2.29, 1.57, 1.08 Å) (Figure S1g).

After the removal of MeOH, a seven-membered cyclic ketone **A** is located as new starting point of the following three steps. Then one hydrogen atom H7 of methylene undergoes two times of proton migration arriving active α-C of indole. From **A**, H7 moves from to C8 to C10 via **ts-Ain2** with activation energy of 32.5 kcal mol^{-1} endothermic by 2.0 kcal mol^{-1} in step 2 and again from C10 to C1 via **ts-in23** with low activation energy of 1.7 kcal mol^{-1} in step 3 leading to **in3** exothermic by -0.9 kcal mol^{-1}. Two transition vectors are both simple corresponding to C8⋯H7⋯C10 and C10⋯H7⋯C1 (1.71, 1.15, 1.19, 1.64 Å) respectively (Figure S1h, Figure S1i). Obviously, this long range relay mechanism of H transfer is feasible at 120 °C. Therefore the carbocation case proposed by experiment may be not necessary.

With C1-H7 in hand, the final β-elimination together with dehydration occurs via **ts-in34** in step 4 with a barrier of 31.9 kcal mol^{-1} exothermic by -3.6 kcal mol^{-1}delivering **in4**. The transition vector is composed of a third proton H7 transfer from C1 to O4, C4⋯O4 separation forming H_2O molecule (1.37, 1.36, 1.85 Å) (Figure S1j). When H_2O is lost from **in4**, the desired **4b** is obtained with new C3-C4 double bond. The Friedel−Crafts acylation is rate-limiting for cycloheptenone fused indole formation. All barriers are readily to overcome under high temperature of experiment.

4 Conclusions

Our DFT calculations provide the first theoretical investigation on Rh(III)-catalyzed cascade reaction of N-alkoxycarbamoyl indole with CF_3–ynone. The cleavage of carbamoyl and indoyl bond gives five-membered rhodacycle via two steps of reversible CMD process. The triple bond is inserted into Rh−C after ynone coordination with Rh(III) and removal of two HCl. After proto-demetalation assisted by one HCl, an extra MeOH is embedded into carbonyl group determined to be rate-limiting. forming N-alkoxycarbamoyl unit The complex is then removed into two parts of indole and N-alkoxycarbamoyl unit indispensable for C−H activation. The intramolecular N-nucleophilic addition of the former affords product pyrrolo[1,2-a]indole and Rh(III) is recovered with a second HCl from the latter both favorable in

thermodynamics.

For cascade transformation to cycloheptenone fused indole without catalyst, the rate-limiting intramolecular Friedel−Crafts acylation is initiated by ester cleavage forming MeOH molecule and seven-membered cyclic ketone. The long range relay of H transfer arriving at α-C of indole is feasible via two steps. The last β-elimination is achieved after dehydration of one H_2O molecule. All barriers are readily to overcome under high temperature of experiment. The positive solvation effect is suggested by decreased absolute and activation energies in MeOH solution compared with in gas. These results are supported by Multiwfn analysis on FMO composition of specific TSs, and MBO value of vital bonding, breaking.

Electronic Supplementary Material

Supplementary data available: [Computation information and cartesian coordinates of stationary points; Calculated relative energies for the ZPE-corrected Gibbs free energies (ΔG_{gas}), and Gibbs free energies (ΔG_{sol}) for all species in solution phase at 353 K.]

Author contributions: Conceptualization, Nan Lu; Methodology, Nan Lu; Software, Nan Lu; Validation, Nan Lu; Formal Analysis, Nan Lu; Investigation, Nan Lu; Resources, Nan Lu; Data Curation, Nan Lu; Writing-Original Draft Preparation, Nan Lu; Writing-Review & Editing, Nan Lu; Visualization, Nan Lu; Supervision, Chengxia Miao; Project Administration, Chengxia Miao; Funding Acquisition, Chengxia Miao. All authors have read and agreed to the published version of the manuscript.

Funding: This work was supported by National Natural Science Foundation of China (21972079) and Key Laboratory of Agricultural Film Application of Ministry of Agriculture and Rural Affairs, P.R. China.

Conflict of interest: The authors declare no conflict of interest.

References

1. Shelke, Y. G.; Hande, P. E.; Gharpure, S. J. (2021). Recent Advances in the Synthesis of Pyrrolo[1,2-a]indoles and Their Derivatives. Org. *Biomol. Chem*.19, 7544−7574.
2. Shan, Y.; Yang, Z.; Yu, J.-T.; Pan, C. (2022). Metal-Free Polychloromethyl Radical-Initiated Cyclization of Unactivated N-Allylindoles towards Pyrrolo[1,2-a]indoles. Org. *Biomol. Chem*.20, 5259−5263.
3. Sindhe, H.; Saiyed, N.; Kamble, A.; Reddy, M. M.; Singh, A.; Sharma, S. (2023). Catalytic and Chemodivergent Synthesis of 1-Substituted 9H-Pyrrolo[1,2-a]indoles via Annulation of β-CF3 Enones with 3-Substituted Indoles. *J. Org. Chem*. 88, 230−244.
4. Zhao, P.; Wang, L.; Guo, X.; Chen, J.; Liu, Y. (2023). Visible Light-Driven α-Diazoketones as Denitrogenated Synthons: Synthesis of Fluorinated N-Heterocycles via Multicomponent Cyclization Reactions. Org. Lett.25, 3314−3318.
5. Wu, Y.; Pi, C.; Wu, Y.; Cui, X. (2021). Directing Group Migration Strategy in Transition-Metal- Catalysed Direct C−H Functionalization. Chem. Soc. Rev. 50, 3677−3689.
6. Song, L.; Van der Eycken, E. V. (2021). Transition Metal-Catalyzed Intermolecular Cascade C−H Activation/Annulation Processes for the Synthesis of Polycycles. *Chem.-Eur*. J. 27, 121−144.
7. Liu, B.; Romine, A. M.; Rubel, C. Z.; Engle, K. M.; Shi, B.-F. (2021). Transition-Metal-Catalyzed, Coordination-Assisted Functionalization of Nonactivated C(sp3)−H Bond. Chem. Rev. 121, 14957−15074.
8. Chen, J.; Zhong, T.; Zheng, X.; Yin, C.; Zhang, L. et al. (2021). Selective Synthesis of Fused Tricyclic [1,3]Oxazino-[3,4-a]indolone and Dihydropyrimido[1,6-a]Indolone via Rh(III)-Catalyzed [3 + 3] or [4 + 2] C−H Annulation. Adv. *Synth. Catal*. 2021, 363, 446−452.
9. Prusty, P.; Jambu, S.; Jeganmohan, M. (2022). Rh(III)-Catalyzed Selective Olefination of N-Carboxamide Indoles with Unactivated Olefins at Room Temperature via an Internal Oxidation. Org. Lett. 24, 1121−1126.
10. Duan, Y.; Lu, S.-N.; Yang, Z.; Chen, Z.; Wu, X.-F. (2023). Rh(III)-Catalyzed C−H Activation/Annulation of N-Carbamoylindoles with CF3-Imidoyl Sulfoxonium Ylides for the Divergent Synthesis of Trifluoromethyl-Substituted (dihydro)-Pyrimidoindolones. Org. Chem. Front., 10, 3843−3848.
11. Wang, J.; Ba, D.; Yang, M.; Cheng, G.; Wang, L. (2021). Regioselective Synthesis of 2,4-Diaryl-6-trifluoromethylated Pyridines through Copper-Catalyzed Cyclization of CF3-Ynones and Vinyl Azides. *J. Org. Chem*. 86, 6423−6432.
12. Huang, H.; Wang, H.; Gong, C.; Zhuang, Z.; Feng, W. et al. (2022). Synthesis of 2-Trifluoromethylquinolines through Rhodium-Catalysed Redox-Neutral [3 + 3] Annulation between Anilines and CF3-Ynones using Traceless Directing Groups. Org. *Chem. Front*. 9, 413−419.
13. Li, H.; Shen, M.; Li, B.; Zhang, X.; Fan, X. (2023). Solvent-Dependent Selective Synthesis of CF 3 -Tethered Indazole Derivatives Based on Multiple Bond Activations. *Org. Lett*, 25, 720−725.
14. Wang, M.; Zhang, L.; Chen, X.; Zhang, X.; Fan, X. (2021). An Unusual Reaction Mode of 1-Phenylpyrazolidinones toward Diazonaphthalen-2(1H)-ones Featuring Cascade C(sp2)−H and C(sp3)−H Bond Cleavage. Org. Chem. Front., 8, 3238−3243.
15. Shen, M.; Li, H.; Zhang, X.; Fan, X. (2022). Rh(III)-Catalyzed Simultaneous [3 + 3]/[5 + 1] Annulation of 1-Arylpyrazolidinones with gem-Difluorocyclopropenes Leading to Fluorinated Pyridopyrimidinone Derivatives. Org. Chem. Front.9, 5976−5982.
16. Song, X.; Wang, K.; Zhang, X.; Fan, X. (2023). Unsymmetrical Relay C−H Alkenylation and [2 + 2] Cycloaddition of N-Arylsydnones with Allenyl Acetates Leading to Quinoline-Fused Cyclobutanes. Org. Chem. Front, 10, 1191−1197.
17. Zhou, Q.; Song, X.; Zhang, X.; Fan, X. (2022). Synthesis of Spiro[benzo[d][1,3]oxazine-4,4'-isoquinoline]s via [4 + 1 + 1] Annulation of N-Aryl Amidines with Diazo Homophthalimides and O2. Org. Lett. 24, 1280−1285.
18. Yu, C.; Xu, Y.; Zhang, X.; Fan, X. Synthesis of N-Arylindoles from 2-Alkenylanilines and Diazonaphthalen-2(1H)-ones through Simultaneous Indole Construction and Aryl Introduction. *J. Org. Chem*., 87, 7392−7404.
19. Wang, K.; Song, X.; Xin, Y.; Zhang, X.; Fan, X. (2023). Condition-Controlled Selective Synthesis of Pyranone-Tethered Indazoles or Carbazoles through the Cascade Reactions of N-Nitrosoanilines with Iodonium Ylides. Org. Lett.25, 4422−4428.
20. Yu, C.; Xu, Y.; Zhang, X.; Fan, X. (2022). Synthesis of Pyrazolonyl Spirodihydroquinolines or Pyrazolonyl Spiroindolines under Aerobic or Anaerobic Conditions. Org. Lett. 24, 9473−9478.
21. Ghosh, P.; Das, S. (2021). The C−H Functionalization of N-Alkoxycarbamoyl Indoles by Transition Metal Catalysis. Org. Biomol. Chem. 19, 7949−7969.
22. Nipate, D. S.; Meena, N.; Swami, P. N.; Rangan, K.; Kumar, A. (2024). Rh(III)-catalyzed Oxidative [4+2] Annulation of 2-Arylquinoxalines and 2-Aryl-2H-Indazoles with Allyl Alcohols. Chem. Commun. 60, 344−347.

23. Li, X.; Liu, J. Song, R.; Luo, X.; Luo, H. (2024). Rhodium(III)-Catalyzed Switchable β-C(sp2)–H Alkenylation and Alkylation of Acyclic Enamides with Allyl Alcohols. Org. Lett. 26 (17), 3673-3678.
24. Wang, M.; Yan, S.; Li, B.; Hou, H.; Ma, C. et al. (2024). Synthesis of CF3-Substituted N-Heterocyclic Compounds Based on C−H Activation-Initiated Formal [2 + 3] Annulation Featuring with a Latent Nucleophilic Site. *J. Org. Chem*. https://doi.org/10.1021/acs.joc.4c00508
25. Zhan, S.-C.; Sun, J.; Sun, Q.; Han, Y.; Yan, C.-G. (2023). Acid-Modulated Construction of Cyclopenta[b]indole and Cyclohepta[b]indole via Unprecedented C3/C2 Carbocation Rearrangement. J. Org. Chem.88, 5440−5456.
26. Frisch, M. J.; Trucks, G. W.; Schlegel, H. B. et al. (2010). Gaussian 09 (Revision B.01), Gaussian, Inc., Wallingford, CT,.
27. Hay, P. J.; Wadt, W. R. (1985). Ab initio effective core potentials for molecular calculations-potentials for the transition-metal atoms Sc to Hg. *J. Chem*. Phys., 82, 270-283.
28. Lv, H.; Han, F.; Wang, N.; Lu, N.; Song, Z. et al. (2022). Ionic Liquid Catalyzed C-C Bond Formation for the Synthesis of Polysubstituted Olefins. *Eur. J. Org. Chem*, e202201222.
29. Zhuang, H.; Lu, N.; Ji, N.; Han, F.; Miao, C. (2021). Bu4NHSO4-Catalyzed Direct N-Allylation of Pyrazole and its Derivatives with Allylic Alcohols in Water: A Metal-free, Recyclable and Sustainable System. Advanced Synthesis & Catalysis, 363, 5461-5472.
30. Lu, N.; Lan, X.; Miao, C.; Qian, P. (2020). Theoretical investigation on transformation of Cr(II) to Cr(V) complexes bearing tetra-NHC and group transfer reactivity. Int. J. Quantum Chem, 120, e26340.
31. Lu, N.; Liang, H.; Qian, P.; Lan, X.; Miao, C. (2020). Theoretical investigation on the mechanism and enantioselectivity of organocatalytic asymmetric Povarov reactions of anilines and aldehydes. Int. *J. Quantum Chem*. 120, e26574.
32. Lu, N.; Wang, Y. (2023). Alloy and Media Effects on the Ethanol Partial Oxidation Catalyzed by Bimetallic Pt6M (M= Co, Ni, Cu, Zn, Ru, Rh, Pd, Sn, Re, Ir, and Pt). Computational and Theoretical Chemistry, 1228, 114252.
33. Becke, A. D. (1996). Density-functional thermochemistry. IV. A new dynamical correlation functional and implications for exact-exchange mixing. *J. Chem. Phys*, 104, 1040-1046.
34. Lee, C. T.; Yang,W. T.; Parr, R. G. (1988). Development of the Colle-Salvetti correlation-energy formula into a functional of the electron density. Phys. Rev. B, 37, 785-789.
35. Catellani, M.; Mealli, C.; Motti, E.; Paoli, P.; Perez-Carren˜o, E. et al. (2002). Palladium-Arene Interactions in Catalytic Intermediates: An Experimental and Theoretical Investigation of the Soft Rearrangement between η1 and η2 Coordination Modes. *J. AM. CHEM*. SOC, 124, 4336-4346.
36. Zicovich-Wilson, C. M.; Pascale, F.; Roetti, C.; Saunders, V. R.; Dovesi, R. (2004). Calculation of the Vibration Frequencies of α-Quartz: The Effect of Hamiltonian and Basis Set. J. Comput. Chem, 25, 1873–1881.
37. Nielsen, R. J., Goddard III, W. A. (2006). Mechanism of the Aerobic Oxidation of Alcohols by Palladium Complexes of N-Heterocyclic Carbenes. *J. AM. CHEM*. SOC.128, 9651-9660.
38. Zandler, M. E.; D'Souza, F. (2006). The remarkable ability of B3LYP/3-21G(*) calculations to describe geometry, spectral and electrochemical properties of molecular and supramolecular porphyrin–fullerene conjugates. 9, 960–981.
39. Marenich, A. V.; Cramer, C. J.; Truhlar, D. G. (2009). Universal Solvation Model Based on Solute Electron Density and on a Continuum Model of the Solvent Defined by the Bulk Dielectric Constant and Atomic Surface Tensions. *J. Phys. Chem*. B, 113, 6378–6396.
40. Tapia, O. (1992). Solvent effect theories: Quantum and classical formalisms and their applications in chemistry and biochemistry. *J. Math. Chem*. 10, 139-181.
41. Tomasi, J.; Persico, M.(1994). Molecular Interactions in Solution: An Overview of Methods Based on Continuous Distributions of the Solvent. Chem. Rev. 94, 2027-2094.
42. Tomasi, J.; Mennucci, B.; Cammi, R. (2005). Quantum Mechanical Continuum Solvation Models. Chem. Rev., 105, 2999-3093.
43. Reed, A. E.; Weinstock, R. B.; Weinhold, F. (1985). Natural population analysis. *J. Chem. Phys*. 83, 735-746.
44. Reed, A. E.; Curtiss, L. A.; Weinhold, F. (1988). Intermolecular interactions from a natural bond orbital donor-acceptor view point. Chem. Rev. 88, 899-926.
45. Lu, T.; Chen, F. (2012). Multiwfn: A multifunctional wavefunction analyzer. *J. Comput. Chem*. 33, 580-592.

Software: GAUSSIAN09

Level of Theory: B3LYP

Basis Set: genecp

Geometry [Cartesian coordinates]:

Optimized Cartesian coordinates for **ts- i01**

Center Number	Atomic Number	Atomic Type	Coordinates (Angstroms) X	Y	Z
1	6	0	2.800596	-2.739528	-2.368211
2	6	0	2.378712	-2.848235	-1.027683
3	6	0	1.328650	-2.084151	-0.528144
4	6	0	0.712160	-1.199522	-1.414207
5	6	0	1.109615	-1.079225	-2.768300
6	6	0	2.174927	-1.862543	-3.243962
7	7	0	-0.370425	-0.328679	-1.218145
8	6	0	-0.612774	0.345550	-2.427886
9	6	0	0.268835	-0.083059	-3.387504
10	6	0	-1.182182	-0.334552	-0.077597
11	7	0	-2.593166	-0.412834	-0.422039
12	6	0	0.403860	0.449455	-4.780293
13	8	0	-0.763314	-0.404842	1.050085
14	1	0	3.626361	-3.352702	-2.717534
15	1	0	2.888657	-3.540943	-0.364427
16	1	0	1.012512	-2.155665	0.505487
17	1	0	2.498798	-1.785204	-4.278232
18	1	0	-1.170948	1.275748	-2.420311
19	1	0	-2.774739	-1.415976	-0.824836
20	1	0	-0.290414	1.276833	-4.960661
21	1	0	0.204704	-0.330621	-5.526965
22	1	0	1.419029	0.820225	-4.968863
23	8	0	-3.424529	-0.215710	0.710529
24	6	0	-3.522931	-1.385005	1.560107
25	1	0	-2.579856	-1.564279	2.078806
26	1	0	-4.299144	-1.110632	2.278376
27	1	0	-3.822334	-2.262042	0.979665
28	45	0	-3.433094	0.797211	-2.014900
29	6	0	-5.057990	-0.600220	-2.579821
30	6	0	-5.564662	0.642532	-2.032928
31	6	0	-4.323455	-0.324457	-3.759713
32	1	0	-5.095945	-1.577242	-2.106839
33	6	0	-5.178628	1.690981	-2.962335
34	6	0	-4.399409	1.124842	-3.999476
35	1	0	-5.376484	2.746785	-2.826597
36	6	0	-6.418981	0.795616	-0.818474
37	1	0	-6.371568	1.815569	-0.428489
38	1	0	-7.463596	0.566290	-1.069676
39	1	0	-6.095383	0.106215	-0.034568
40	6	0	-3.795471	1.859880	-5.154037
41	1	0	-2.813924	1.456760	-5.419161
42	1	0	-4.440412	1.758807	-6.037319
43	1	0	-3.687345	2.924484	-4.930599
44	6	0	-3.629628	-1.338896	-4.608553
45	1	0	-2.763306	-0.914987	-5.124056
46	1	0	-3.309341	-2.181678	-3.986262
47	1	0	-4.324685	-1.712756	-5.373363
48	17	0	-3.184104	-3.146699	-1.512459
49	17	0	-2.673727	2.788415	-0.962212

Optimized Cartesian coordinates for **ts- i12**

Center Number	Atomic Number	Atomic Type	Coordinates (Angstroms) X	Y	Z
1	6	0	-5.597485	-0.117171	-0.607095
2	6	0	-5.278098	1.196783	-0.193365
3	6	0	-3.996720	1.552518	0.210553
4	6	0	-3.023147	0.546726	0.187043
5	6	0	-3.315045	-0.778928	-0.242313
6	6	0	-4.630024	-1.107596	-0.632093
7	7	0	-1.684152	0.580959	0.526627
8	6	0	-1.086980	-0.696092	0.330664
9	6	0	-2.104229	-1.535739	-0.168618
10	6	0	-0.885050	1.721578	0.707929
11	7	0	0.450933	1.343332	0.614774
12	6	0	-1.969370	-3.006979	-0.390756
13	8	0	-1.312885	2.846826	0.900488
14	1	0	-6.615863	-0.347093	-0.906483
15	1	0	-6.060446	1.950813	-0.184912
16	1	0	-3.748045	2.554715	0.534894
17	1	0	-4.875968	-2.116344	-0.951779
18	1	0	-0.698125	-1.265075	1.463817
19	1	0	1.197146	3.611864	-0.682420
20	1	0	-1.427882	-3.456600	0.451232
21	1	0	-1.410406	-3.231539	-1.308039
22	1	0	-2.945690	-3.493632	-0.470582
23	8	0	1.343095	2.422595	0.692666
24	6	0	1.549951	2.848112	2.053348
25	1	0	1.916296	2.006830	2.650612
26	1	0	2.308688	3.631815	1.992311
27	1	0	0.623984	3.247257	2.473330
28	45	0	0.980594	-0.439780	-0.029132
29	6	0	3.218720	-0.584930	-0.257489
30	6	0	2.728912	-1.779693	0.382475
31	6	0	2.612022	-0.462419	-1.531507
32	1	0	3.887589	0.135974	0.194216
33	6	0	1.847919	-2.431167	-0.549339
34	6	0	1.746729	-1.635163	-1.721993
35	1	0	1.311734	-3.350649	-0.356813
36	6	0	3.110497	-2.281501	1.736420
37	1	0	2.228852	-2.638488	2.277745
38	1	0	3.822247	-3.112114	1.632308
39	1	0	3.587949	-1.495649	2.328101
40	6	0	1.003230	-1.967497	-2.977918
41	1	0	0.529020	-1.083778	-3.414813
42	1	0	1.695755	-2.376877	-3.726165
43	1	0	0.229977	-2.717800	-2.794265
44	6	0	2.849439	0.624698	-2.531814
45	1	0	3.615771	0.308859	-3.252996
46	1	0	1.942439	0.863414	-3.094052
47	1	0	3.192761	1.542042	-2.047298
48	17	0	1.365443	4.300755	-1.789277
49	17	0	-0.360227	-2.108013	2.865499

Optimized Cartesian coordinates for **ts-IIIII**

Center Number	Atomic Number	Atomic Type	Coordinates (Angstroms) X	Y	Z
1	6	0	-5.246464	-2.620468	1.134053
2	6	0	-4.669396	-2.597946	2.422360
3	6	0	-3.361474	-2.172894	2.630566
4	6	0	-2.636794	-1.765827	1.503965
5	6	0	-3.190730	-1.793565	0.195221
6	6	0	-4.520019	-2.223703	0.019791
7	7	0	-1.340348	-1.286909	1.385155

8	6	0	-1.055892	-1.025489	0.034322
9	6	0	-2.184372	-1.326379	-0.721210
10	6	0	-0.302848	-1.392190	2.355596
11	7	0	0.870829	-1.028835	1.779044
12	6	0	-2.392679	-1.169368	-2.195122
13	8	0	-0.512875	-1.727488	3.514868
14	1	0	-6.273203	-2.956702	1.016507
15	1	0	-5.262177	-2.919533	3.274545
16	1	0	-2.904234	-2.155174	3.611297
17	1	0	-4.967035	-2.248025	-0.970774
18	1	0	-1.542256	-0.678582	-2.673114
19	1	0	-3.284323	-0.566010	-2.408682
20	1	0	-2.543298	-2.141972	-2.684200
21	8	0	2.001527	-1.284536	2.558249
22	6	0	2.228563	-0.239932	3.511647
23	1	0	1.395579	-0.184885	4.217874
24	1	0	3.144824	-0.527782	4.034809
25	1	0	2.375136	0.725192	3.015659
26	45	0	1.010697	-0.861123	-0.296413
27	6	0	2.779188	-0.743500	-1.766822
28	6	0	3.158528	-1.522596	-0.642893
29	6	0	1.703782	-1.388760	-2.466012
30	1	0	3.212269	0.213874	-2.030674
31	6	0	2.289275	-2.684333	-0.649133
32	6	0	1.427680	-2.628456	-1.777285
33	1	0	2.312323	-3.480632	0.084969
34	6	0	4.293341	-1.259810	0.298273
35	1	0	4.026611	-1.570164	1.311171
36	1	0	5.184616	-1.820076	-0.015062
37	1	0	4.540172	-0.194862	0.316979
38	6	0	0.459291	-3.695016	-2.194584
39	1	0	-0.442148	-3.274987	-2.647234
40	1	0	0.922755	-4.362404	-2.933672
41	1	0	0.154536	-4.304131	-1.338838
42	6	0	1.143675	-0.952086	-3.788541
43	1	0	1.787550	-1.300268	-4.607942
44	1	0	0.144715	-1.358777	-3.965273
45	1	0	1.085761	0.138757	-3.859095
46	6	0	-0.376201	0.986087	-0.317488
47	6	0	0.801544	1.144279	0.172238
48	6	0	1.764830	2.106313	0.638794
49	8	0	2.973126	2.033011	0.488177
50	6	0	1.164906	3.314387	1.405238
51	9	0	2.104642	4.217173	1.693597
52	9	0	0.603323	2.897284	2.558044
53	9	0	0.205531	3.915702	0.670422
54	6	0	-1.407262	1.713160	-1.046890
55	6	0	-1.034455	2.455221	-2.182673
56	6	0	-1.977035	3.230608	-2.855188
57	6	0	-3.294076	3.286627	-2.394001
58	6	0	-3.666636	2.562074	-1.258086
59	6	0	-2.733889	1.772074	-0.589561
60	1	0	-0.005085	2.418981	-2.526691
61	1	0	-1.680877	3.794803	-3.735138
62	1	0	-4.027566	3.894998	-2.915839
63	1	0	-4.687428	2.612098	-0.890135
64	1	0	-3.022745	1.205898	0.288683

Optimized Cartesian coordinates for **ts-i3IV**

Center Number	Atomic Number	Atomic Type	Coordinates (Angstroms) X	Y	Z
1	6	0	3.606719	4.922223	0.232129
2	6	0	4.199187	4.006682	-0.668901

3	6	0	3.537777	2.861023	-1.086321
4	6	0	2.250905	2.633766	-0.572147
5	6	0	1.634733	3.545707	0.319521
6	6	0	2.332530	4.703391	0.725407
7	7	0	1.385184	1.572870	-0.772610
8	6	0	0.190712	1.826883	-0.074819
9	6	0	0.334162	3.041644	0.619596
10	6	0	1.807310	0.505355	-1.676677
11	7	0	1.924696	-0.688761	-1.046934
12	6	0	-0.598638	3.745093	1.566776
13	8	0	2.204511	0.800833	-2.793637
14	1	0	4.157796	5.810278	0.528869
15	1	0	5.195883	4.209585	-1.051451
16	1	0	3.979008	2.181672	-1.804747
17	1	0	1.873074	5.415133	1.405709
18	1	0	-1.211894	3.057193	2.151570
19	1	0	-1.286810	4.421062	1.044480
20	1	0	-0.016416	4.350835	2.269621
21	8	0	2.474256	-1.678563	-1.907150
22	6	0	3.893300	-1.577648	-1.936909
23	1	0	4.321696	-1.641963	-0.926408
24	1	0	4.227847	-2.430889	-2.533803
25	1	0	4.211848	-0.647222	-2.418595
26	45	0	0.667969	-1.683742	0.267323
27	6	0	0.094103	-3.058579	1.962892
28	6	0	1.307793	-3.606152	1.382791
29	6	0	0.376270	-1.771686	2.491368
30	1	0	-0.863694	-3.557943	2.008116
31	6	0	2.314636	-2.627803	1.508734
32	6	0	1.748360	-1.446829	2.132472
33	1	0	3.324230	-2.707871	1.127579
34	6	0	1.435071	-4.954313	0.746185
35	1	0	2.335513	-5.019536	0.129574
36	1	0	1.491190	-5.730467	1.520988
37	1	0	0.566986	-5.175268	0.117545
38	6	0	2.510850	-0.222309	2.535460
39	1	0	3.315883	-0.014443	1.826167
40	1	0	1.865634	0.659438	2.579185
41	1	0	2.957556	-0.364382	3.529338
42	6	0	-0.545405	-0.921158	3.308333
43	1	0	-0.341963	-1.080320	4.376144
44	1	0	-0.402995	0.143441	3.101605
45	1	0	-1.584997	-1.186099	3.108617
46	6	0	-0.988091	0.971843	-0.070874
47	6	0	-1.017874	-0.409045	-0.161337
48	6	0	-2.341287	-1.102565	0.024030
49	8	0	-2.596228	-1.879285	0.925971
50	6	0	-3.446105	-0.984760	-1.080609
51	9	0	-4.596920	-0.525704	-0.558022
52	9	0	-3.687384	-2.207744	-1.582728
53	9	0	-3.093625	-0.180198	-2.099362
54	6	0	-2.274558	1.724742	0.097130
55	6	0	-3.156493	1.470185	1.159647
56	6	0	-4.345577	2.191211	1.284949
57	6	0	-4.678487	3.161310	0.340577
58	6	0	-3.811998	3.416587	-0.727766
59	6	0	-2.615227	2.714839	-0.841906
60	1	0	-2.901398	0.724382	1.905195
61	1	0	-5.010458	1.989628	2.120108
62	1	0	-5.607872	3.716513	0.432585
63	1	0	-4.070215	4.164739	-1.472118
64	1	0	-1.940393	2.917408	-1.667965
65	17	0	-0.421798	-2.573268	-2.036703
66	1	0	-0.668368	-1.253455	-1.363079

Optimized Cartesian coordinates for **ts-i45**

Center Number	Atomic Number	Atomic Type	Coordinates (Angstroms) X	Y	Z
1	6	0	-1.966571	2.002584	-3.738131
2	6	0	-2.480820	1.490353	-2.528357
3	6	0	-2.166700	0.207162	-2.090213
4	6	0	-1.328512	-0.564789	-2.900214
5	6	0	-0.759485	-0.049821	-4.086885
6	6	0	-1.102050	1.244996	-4.517195
7	7	0	-0.859119	-1.867158	-2.726801
8	6	0	0.081817	-2.132525	-3.755707
9	6	0	0.140554	-1.046040	-4.607994
10	6	0	-0.893332	-2.548267	-1.478487
11	7	0	-2.128652	-2.913155	-1.040653
12	6	0	0.926327	-0.889758	-5.876312
13	8	0	0.185081	-3.236674	-1.127985
14	1	0	-2.235995	3.007714	-4.050201
15	1	0	-3.126595	2.116034	-1.917762
16	1	0	-2.547614	-0.182585	-1.154461
17	1	0	-0.681128	1.650982	-5.433082
18	1	0	1.387567	-1.824535	-6.198398
19	1	0	1.730511	-0.153046	-5.750367
20	1	0	0.283895	-0.527958	-6.689144
21	8	0	-1.986951	-3.501092	0.228261
22	6	0	-2.902091	-2.942163	1.168666
23	1	0	-3.939096	-3.150745	0.889491
24	1	0	-2.675197	-3.458796	2.104302
25	1	0	-2.739437	-1.865777	1.289091
26	45	0	-3.800104	-3.434561	-2.150438
27	6	0	-5.800734	-3.412523	-3.031305
28	6	0	-5.301642	-2.062643	-2.966114
29	6	0	-4.956980	-4.176498	-3.882855
30	1	0	-6.618899	-3.806477	-2.442643
31	6	0	-4.172089	-1.985658	-3.858232
32	6	0	-3.957319	-3.261790	-4.436568
33	1	0	-3.587007	-1.097768	-4.048537
34	6	0	-5.908332	-0.928578	-2.205431
35	1	0	-6.361916	-1.273067	-1.271287
36	1	0	-5.162011	-0.161345	-1.984057
37	1	0	-6.699296	-0.464246	-2.810482
38	6	0	-2.969609	-3.598840	-5.504224
39	1	0	-2.588003	-4.617434	-5.409120
40	1	0	-3.471149	-3.528517	-6.480455
41	1	0	-2.128564	-2.901453	-5.507557
42	6	0	-5.112225	-5.625211	-4.225224
43	1	0	-5.668005	-5.730320	-5.167101
44	1	0	-4.142803	-6.115386	-4.346386
45	1	0	-5.658106	-6.147848	-3.436623
46	6	0	0.740950	-3.443156	-3.927402
47	6	0	-0.031560	-4.565012	-3.827453
48	6	0	0.357226	-5.971230	-3.835119
49	8	0	1.454373	-6.472309	-4.007990
50	6	0	-0.853838	-6.925811	-3.619285
51	9	0	-1.703366	-6.819563	-4.691809
52	9	0	-1.567151	-6.601026	-2.527066
53	9	0	-0.476505	-8.198102	-3.527377
54	6	0	2.197559	-3.394516	-4.198434
55	6	0	2.815304	-4.190711	-5.177877
56	6	0	4.183765	-4.083227	-5.413867
57	6	0	4.961459	-3.196723	-4.664194
58	6	0	4.360190	-2.405106	-3.683451
59	6	0	2.987335	-2.490757	-3.462164
60	1	0	2.222146	-4.886889	-5.757741

61	1	0	4.645265	-4.698683	-6.181021
62	1	0	6.030633	-3.123656	-4.844617
63	1	0	4.958436	-1.717096	-3.092571
64	1	0	2.519406	-1.872786	-2.701996
65	17	0	-4.329581	-5.249920	-0.722335
66	1	0	-1.082350	-4.406004	-3.615246
67	8	0	0.036079	-1.056071	-0.432812
68	1	0	0.641026	-2.424800	-0.648504
69	6	0	-0.273163	-0.661784	0.862670
70	1	0	-0.356901	-1.501452	1.576720
71	1	0	0.512293	0.013621	1.248958
72	1	0	-1.218721	-0.088314	0.911673

Optimized Cartesian coordinates for **ts-i56**

Center Number	Atomic Number	Atomic Type	Coordinates (Angstroms) X	Y	Z
1	6	0	0.587046	3.202410	-1.737695
2	6	0	-0.173876	2.726244	-0.642001
3	6	0	-0.536336	1.394200	-0.526222
4	6	0	-0.135400	0.489371	-1.535708
5	6	0	0.641300	0.970796	-2.639016
6	6	0	1.002706	2.332896	-2.728540
7	7	0	-0.304901	-0.874289	-1.630881
8	6	0	0.353303	-1.263283	-2.809377
9	6	0	0.948615	-0.152654	-3.451308
10	6	0	-1.990594	-1.805352	-0.862770
11	7	0	-2.678373	-2.507565	-1.787629
12	6	0	1.875882	-0.081553	-4.633504
13	8	0	-1.329934	-2.554296	0.034897
14	1	0	0.853324	4.254965	-1.787324
15	1	0	-0.470109	3.423793	0.137840
16	1	0	-1.101253	1.053160	0.330982
17	1	0	1.603047	2.689420	-3.562264
18	1	0	1.344190	0.131759	-5.570360
19	1	0	2.433014	-1.007689	-4.789251
20	1	0	2.604827	0.723972	-4.486495
21	8	0	-3.695207	-1.714340	-2.394402
22	6	0	-3.201273	-0.929216	-3.480944
23	1	0	-2.787094	-1.569988	-4.269019
24	1	0	-4.078286	-0.397159	-3.861250
25	1	0	-2.447420	-0.210731	-3.149626
26	45	0	-3.121379	-4.512168	-2.085016
27	6	0	-4.545323	-6.116455	-2.421692
28	6	0	-5.095992	-4.846053	-2.863930
29	6	0	-3.401794	-6.424718	-3.197859
30	1	0	-4.899369	-6.684902	-1.571527
31	6	0	-4.298372	-4.421071	-3.984765
32	6	0	-3.252531	-5.357737	-4.192988
33	1	0	-4.440385	-3.504380	-4.540405
34	6	0	-6.312529	-4.162952	-2.330720
35	1	0	-6.199460	-3.076662	-2.393253
36	1	0	-7.192872	-4.451947	-2.921105
37	1	0	-6.496380	-4.441405	-1.289319
38	6	0	-2.213702	-5.319644	-5.261194
39	1	0	-2.396960	-6.139578	-5.969872
40	1	0	-2.239696	-4.376591	-5.810642
41	1	0	-1.210513	-5.454914	-4.843640
42	6	0	-2.510727	-7.617905	-3.056222
43	1	0	-2.692361	-8.321553	-3.880206
44	1	0	-1.455343	-7.328340	-3.082010
45	1	0	-2.704930	-8.132795	-2.112208
46	6	0	0.539639	-2.657398	-3.169042
47	6	0	0.626228	-3.615958	-2.175549

48	6	0	0.604372	-5.049803	-2.312678
49	8	0	0.277634	-5.733180	-3.288079
50	6	0	1.094941	-5.850169	-1.076560
51	9	0	0.446879	-7.019286	-0.967251
52	9	0	0.966624	-5.188092	0.089337
53	9	0	2.413027	-6.124865	-1.241020
54	6	0	0.726096	-2.981227	-4.609959
55	6	0	-0.088384	-2.384563	-5.586814
56	6	0	0.094227	-2.660638	-6.942575
57	6	0	1.109377	-3.528377	-7.348380
58	6	0	1.940538	-4.114496	-6.388588
59	6	0	1.749573	-3.846081	-5.035843
60	1	0	-0.857835	-1.687200	-5.273488
61	1	0	-0.548635	-2.188564	-7.681343
62	1	0	1.261035	-3.738175	-8.403895
63	1	0	2.743250	-4.779139	-6.696089
64	1	0	2.405298	-4.296179	-4.298118
65	17	0	-2.625459	-5.265487	0.093612
66	1	0	0.678772	-3.259466	-1.157884
67	8	0	-2.511752	-0.629730	-0.416283
68	1	0	-0.569624	-2.011711	0.311684
69	6	0	-3.659976	-0.799278	0.439680
70	1	0	-3.839745	0.183899	0.878071
71	1	0	-4.527018	-1.112333	-0.147454
72	1	0	-3.448147	-1.528391	1.227795

Optimized Cartesian coordinates for **ts-i78**

Center Number	Atomic Number	Atomic Type	Coordinates (Angstroms) X	Y	Z
1	6	0	-1.867302	-0.935181	0.500640
2	7	0	-1.684445	0.452377	0.224282
3	8	0	-0.843099	-1.616945	0.380164
4	8	0	-2.807602	0.956611	-0.487950
5	6	0	-2.529974	2.287662	-0.925856
6	1	0	-1.684835	2.284307	-1.622720
7	1	0	-3.438690	2.597796	-1.445639
8	1	0	-2.338450	2.946256	-0.071426
9	45	0	0.383334	0.093122	-0.495512
10	6	0	2.046999	1.302572	-1.116415
11	6	0	1.539544	1.886034	0.096882
12	6	0	2.539130	-0.025317	-0.842399
13	1	0	2.052185	1.782153	-2.087012
14	6	0	1.677574	0.890469	1.125180
15	6	0	2.313128	-0.266550	0.566901
16	1	0	1.316052	1.003432	2.140589
17	6	0	0.996665	3.265330	0.280068
18	1	0	0.599398	3.665981	-0.657171
19	1	0	0.220253	3.272195	1.052975
20	1	0	1.809105	3.927315	0.609946
21	6	0	2.605726	-1.536082	1.309504
22	1	0	3.417536	-2.095659	0.837062
23	1	0	2.888887	-1.313879	2.342771
24	1	0	1.720858	-2.182709	1.340922
25	6	0	3.208843	-0.935643	-1.824938
26	1	0	3.088173	-1.985789	-1.545871
27	1	0	2.780571	-0.803384	-2.822006
28	1	0	4.283970	-0.717679	-1.876853
29	17	0	-0.462232	-0.413377	-2.666895
30	8	0	-3.004557	-1.453475	0.871397
31	6	0	-4.078651	-0.630238	1.419192
32	1	0	-4.625786	-1.308308	2.073270
33	1	0	-3.664413	0.204699	1.988160
34	1	0	-4.708299	-0.278064	0.603838

35	17	0	-1.402306	1.917129	2.747639
36	1	0	-1.579166	1.022175	1.174101

Software: GAUSSIAN09

Level of Theory: M06-2X

Basis Set: 6-31G(d)

Geometry [Cartesian coordinates]:

Optimized Cartesian coordinates for **ts-V3a**

Center Number	Atomic Number	Atomic Type	Coordinates (Angstroms) X	Y	Z
1	6	0	-4.202941	-2.275638	0.752314
2	6	0	-4.564691	-1.043512	0.197334
3	6	0	-3.601376	-0.163226	-0.294383
4	6	0	-2.283064	-0.563668	-0.178798
5	6	0	-1.892946	-1.797551	0.357861
6	6	0	-2.869448	-2.669379	0.835332
7	7	0	-1.102179	0.085261	-0.661003
8	6	0	0.009592	-0.743808	-0.270216
9	6	0	-0.427457	-1.878650	0.322019
10	6	0	0.357886	-2.983758	0.950026
11	1	0	-4.978403	-2.939447	1.121225
12	1	0	-5.612608	-0.767018	0.146561
13	1	0	-3.856630	0.794312	-0.734251
14	1	0	-2.598633	-3.632322	1.258562
15	1	0	0.239973	-3.916459	0.386163
16	1	0	-0.007187	-3.168644	1.965873
17	1	0	1.421347	-2.746120	1.002394
18	6	0	1.219664	0.079573	-0.374311
19	6	0	0.862292	1.372534	-0.482334
20	6	0	-0.641318	1.608291	-0.583598
21	8	0	-1.106047	2.023308	-1.749923
22	6	0	-1.213180	2.270630	0.671731
23	9	0	-0.610741	3.446945	0.879627
24	9	0	-1.005295	1.505590	1.755652
25	9	0	-2.524463	2.485827	0.567021
26	6	0	2.589267	-0.466023	-0.365971
27	6	0	3.634635	0.245147	0.231833
28	6	0	4.930890	-0.256916	0.208055
29	6	0	5.198121	-1.476711	-0.409676
30	6	0	4.162437	-2.193046	-1.004969
31	6	0	2.865560	-1.691511	-0.982764
32	1	0	3.420313	1.185195	0.732267
33	1	0	5.733189	0.300768	0.681047
34	1	0	6.210061	-1.869246	-0.424109
35	1	0	4.364906	-3.141894	-1.491956
36	1	0	2.057154	-2.241609	-1.458243
37	1	0	1.541563	2.204287	-0.631769
38	1	0	-1.193459	0.580463	-1.753035

Optimized Cartesian coordinates for **ts-3bin1**

Center Number	Atomic Number	Atomic Type	Coordinates (Angstroms) X	Y	Z
1	6	0	3.077191	3.748254	-0.460062
2	6	0	3.993913	2.761576	-0.054706
3	6	0	3.602431	1.448961	0.156315
4	6	0	2.255275	1.146845	-0.044453
5	6	0	1.308572	2.128511	-0.436371
6	6	0	1.740336	3.443410	-0.652967

7	7	0	1.554613	-0.035067	0.078764
8	6	0	0.212600	0.185080	-0.163896
9	6	0	0.014914	1.491008	-0.499978
10	6	0	1.789985	-1.326675	0.654631
11	6	0	0.392351	-1.916620	0.645191
12	6	0	-0.516054	-1.053497	0.141405
13	8	0	2.388056	-1.171657	1.915055
14	6	0	2.736301	-2.163406	-0.218150
15	9	0	2.944223	-3.350238	0.390327
16	9	0	3.923997	-1.573123	-0.367410
17	9	0	2.233691	-2.401025	-1.425751
18	1	0	3.425737	4.763675	-0.619184
19	1	0	5.033508	3.033564	0.098648
20	1	0	4.302411	0.687758	0.478405
21	1	0	1.037951	4.212533	-0.963364
22	1	0	0.214247	-2.923903	1.000513
23	1	0	2.526103	-2.055113	2.290905
24	6	0	-1.310064	2.137378	-0.713244
25	1	0	-1.225897	3.230182	-0.649837
26	1	0	-1.774300	1.890285	-1.670173
27	6	0	-1.950722	-1.326201	-0.114299
28	6	0	-2.943006	-0.327289	-0.250391
29	6	0	-2.290128	-2.685593	-0.228785
30	6	0	-4.257558	-0.797628	-0.446494
31	1	0	-3.550136	1.107303	-0.501219
32	6	0	-3.596123	-3.102344	-0.433233
33	1	0	-1.504596	-3.433642	-0.180404
34	6	0	-4.596272	-2.145012	-0.538663
35	1	0	-5.081014	-0.087835	-0.558328
36	1	0	-3.824085	-4.160065	-0.521077
37	1	0	-5.629081	-2.438705	-0.704957
38	6	0	-2.236582	1.749686	0.407746
39	8	0	-2.143384	1.795888	1.579352
40	8	0	-3.743483	2.138794	-0.231117
41	6	0	-4.733170	2.198468	0.802771
42	1	0	-4.549441	3.095432	1.394366
43	1	0	-5.708244	2.255406	0.316769
44	1	0	-4.667305	1.314407	1.442559

Optimized Cartesian coordinates for **ts-Ain2**

Center Number	Atomic Number	Atomic Type	Coordinates (Angstroms) X	Y	Z
1	6	0	-3.325791	3.384970	-0.212057
2	6	0	-4.082672	2.218950	-0.384541
3	6	0	-3.487511	0.963535	-0.432244
4	6	0	-2.104613	0.920184	-0.298838
5	6	0	-1.321723	2.085579	-0.148152
6	6	0	-1.940326	3.328452	-0.097861
7	7	0	-1.222772	-0.161154	-0.296439
8	6	0	0.052091	0.270881	-0.185183
9	6	0	0.115272	1.685668	-0.125433
10	6	0	-1.263459	-1.597589	-0.445768
11	6	0	0.215763	-1.944919	-0.397708
12	6	0	0.973245	-0.821395	-0.258832
13	8	0	-1.944794	-1.913947	-1.629886
14	6	0	-2.019977	-2.236628	0.729828
15	9	0	-2.026091	-3.571333	0.554566
16	9	0	-3.289631	-1.826272	0.778314
17	9	0	-1.448229	-1.965972	1.897406
18	1	0	-3.828303	4.345473	-0.168269
19	1	0	-5.160926	2.294324	-0.481939
20	1	0	-4.064521	0.057489	-0.570194
21	1	0	-1.354089	4.233714	0.027974

22	1	0	0.543499	-2.975450	-0.430398
23	1	0	-1.931056	-2.878147	-1.737088
24	6	0	1.275945	2.462176	0.369547
25	1	0	0.614720	1.949329	-1.123198
26	1	0	1.135169	3.531065	0.466923
27	6	0	2.429814	-0.628744	-0.221940
28	6	0	3.101130	0.577492	0.124427
29	6	0	3.185197	-1.765005	-0.567340
30	6	0	4.507405	0.540396	0.106874
31	6	0	4.565860	-1.761077	-0.576391
32	1	0	2.657958	-2.670284	-0.851182
33	6	0	5.233448	-0.587529	-0.231948
34	1	0	5.012827	1.457057	0.384788
35	1	0	5.113637	-2.655943	-0.854282
36	1	0	6.318543	-0.550847	-0.232524
37	6	0	2.602418	1.988612	0.533156
38	8	0	3.458344	2.758750	0.991676

Optimized Cartesian coordinates for **ts-in23**

Center Number	Atomic Number	Atomic Type	Coordinates (Angstroms) X	Y	Z
1	6	0	-3.243515	3.891878	-0.199304
2	6	0	-4.008617	2.726658	-0.322906
3	6	0	-3.421741	1.465241	-0.331094
4	6	0	-2.039320	1.421768	-0.206646
5	6	0	-1.248602	2.583973	-0.111423
6	6	0	-1.856021	3.830872	-0.098690
7	7	0	-1.163664	0.327130	-0.166838
8	6	0	0.109498	0.749206	-0.083466
9	6	0	0.201237	2.190923	-0.084104
10	6	0	-1.208590	-1.105511	-0.367676
11	6	0	0.270693	-1.459345	-0.327585
12	6	0	1.036522	-0.344293	-0.191023
13	8	0	-1.883344	-1.378528	-1.563680
14	6	0	-1.969654	-1.774438	0.787399
15	9	0	-1.986575	-3.101603	0.567381
16	9	0	-3.235178	-1.353786	0.846873
17	9	0	-1.395139	-1.545571	1.961672
18	1	0	-3.739886	4.856477	-0.186952
19	1	0	-5.087273	2.805375	-0.412716
20	1	0	-4.005606	0.558514	-0.428987
21	1	0	-1.257773	4.732829	-0.017211
22	1	0	0.594571	-2.491274	-0.369137
23	1	0	-1.879742	-2.338738	-1.703465
24	6	0	1.305212	2.957327	0.409401
25	1	0	0.378011	1.898836	-1.225066
26	1	0	1.143289	4.010214	0.601072
27	6	0	2.487272	-0.133481	-0.171057
28	6	0	3.134848	1.080719	0.192189
29	6	0	3.253524	-1.254975	-0.542819
30	6	0	4.541204	1.063096	0.162451
31	6	0	4.633006	-1.227032	-0.565697
32	1	0	2.736274	-2.164087	-0.834957
33	6	0	5.281538	-0.046424	-0.205935
34	1	0	5.032488	1.981658	0.459369
35	1	0	5.194499	-2.106774	-0.863679
36	1	0	6.365980	0.008732	-0.216309
37	6	0	2.616395	2.486703	0.638501
38	8	0	3.471484	3.221735	1.152654

Optimized Cartesian coordinates for **ts-in34**

Center	Atomic	Atomic	Coordinates (Angstroms)

Number	Number	Type	X	Y	Z
1	6	0	1.514807	4.465779	-2.206642
2	6	0	2.792716	3.944971	-1.995127
3	6	0	2.992496	2.751844	-1.301491
4	6	0	1.868497	2.099958	-0.816066
5	6	0	0.565513	2.608917	-1.026994
6	6	0	0.392286	3.797651	-1.723909
7	7	0	1.741731	0.851898	-0.179581
8	6	0	0.388599	0.755711	0.324252
9	6	0	-0.423408	1.697935	-0.415395
10	6	0	2.398477	0.060524	0.714905
11	6	0	1.511332	-1.060485	0.998855
12	6	0	0.232095	-0.611379	0.754226
13	8	0	2.105136	1.174292	2.164199
14	6	0	3.898028	-0.054028	0.768206
15	9	0	4.251730	-0.707101	1.878431
16	9	0	4.496454	1.134486	0.767343
17	9	0	4.348410	-0.744022	-0.284499
18	1	0	1.396813	5.398262	-2.748196
19	1	0	3.656816	4.478189	-2.379013
20	1	0	3.986951	2.352437	-1.149150
21	1	0	-0.604131	4.200232	-1.880632
22	1	0	1.841980	-1.970516	1.478493
23	1	0	1.997440	0.597996	2.936650
24	6	0	-1.766892	1.723870	-0.446397
25	1	0	0.900165	1.199614	1.519228
26	1	0	-2.295342	2.532601	-0.942106
27	6	0	-1.065437	-1.247252	0.972327
28	6	0	-2.320548	-0.623534	0.741130
29	6	0	-1.035107	-2.575608	1.430956
30	6	0	-3.473670	-1.381802	1.004527
31	6	0	-2.188425	-3.299013	1.669391
32	1	0	-0.070319	-3.044450	1.595040
33	6	0	-3.423035	-2.690210	1.455618
34	1	0	-4.429499	-0.900157	0.840382
35	1	0	-2.126269	-4.324530	2.019469
36	1	0	-4.344594	-3.234091	1.637587
37	6	0	-2.677554	0.782050	0.224993
38	8	0	-3.847618	1.123782	0.315909

Table S1. Calculated relative energies (all in kcal mol^{-1}, relative to isolated species) for the ZPE-corrected Gibbs free energies (ΔG_{gas}), Gibbs free energies for all species in solution phase (ΔG_{sol}) at 353 K by B3LYP/6-311++G(d,p)//B3LYP/6-31G(d) method and difference between absolute energy.

Species	ΔG_{gas}	$\Delta G_{sol(MeOH)}$
1a+cprhcl2	0.00	0.00
i0	-183.28	-167.02
ts-i01	-162.00	-154.28
i1	-171.02	-163.45
ts-i12	-148.63	-136.56
i2	-159.02	-147.63
1a+cprhcl2-2hcl	0.00	0.00
I	-99.88	-85.50
1a+cprhcl2-2hcl+2	0.00	0.00
II	-276.10	-253.06
ts-IIIII	-261.61	-241.08
III	-288.08	-270.43
1a+cprhcl2-hcl+2	0.00	0.00
i3	-318.41	-302.09
ts-i3IV	-295.41	-275.44
IV	-338.45	-325.24
1a+cprhcl2-hcl+2+meoh	0.00	0.00

i4	-384.01	-366.65
ts-i45	-350.25	-334.04
i5	-361.43	-341.11
ts-i56	-341.80	-321.02
i6(V+VI)	-395.26	-374.02
V	0.00	0.00
ts-V3a	48.57	41.51
3a	-3.71	-8.19
1a+cprhcl2-hcl+2+meoh-V	0.00	0.00
VI	-113.35	-97.23
1a+cprhcl2+2+meoh-V	0.00	0.00
i7	-146.66	-130.87
ts-i78	-130.54	-117.94
i8	-155.11	-140.01
1a+2+meoh-V	0.00	0.00
VII	-46.22	-46.31
3b	0.00	0.00
ts-3bin1	46.96	42.33
in1	14.91	14.06
3b-meoh	0.00	0.00
A	21.96	19.43
ts-Ain2	60.55	51.90
in2	40.89	21.42
ts-in23	43.64	23.16
in3	34.00	18.54
ts-in34	67.63	50.46
in4	28.36	15.80
3b-meoh-h2o	0.00	0.00
4b	23.51	21.78

Table S2. The activation energy (local barrier) (in kcal mol^{-1}) of all reactions in the gas, solution phase calculated with B3LYP/6-311++G(d,p)//B3LYP/6-31G(d) method.

TS	$\Delta G^{\neq}_{gas}$	$\Delta G^{\neq}_{sol}$
ts-i01 (82i)	21.3	12.7
ts-i12 (396i)	22.4	26.9
ts-IIIII (235i)	14.5	12.0
ts-i3IV (966i)	23.0	26.6
ts-i45 (593i)	33.8	32.6
ts-i56 (193i)	19.6	20.1
ts-i78 (101i)	16.1	12.9
ts-V3a (1615i)	48.6	41.5
ts-3bin1 (974i)	47.0	42.3
ts-Ain2 (873i)	38.6	32.5
ts-in23 (548i)	2.8	1.7
ts-in34 (1762i)	33.6	31.9

Table S3. Mayer bond order (MBO) of typical TSs

	N1⋯H1	H1⋯Cl1	Rh⋯N1	
ts-i01	0.51	0.39	0.39	
	C1⋯H2	H2⋯Cl2	Rh⋯C1	
ts-i12	0.40	0.49	0.58	
	C1⋯C2	Rh⋯C3	C2⋯C3	Rh⋯C1
ts-IIIII	0.34	0.57	1.69	0.59
	Rh⋯C3	Cl3⋯H3	H3⋯C3	Rh⋯Cl3
ts-i3IV	0.60	0.55	0.27	0.45
	C5⋯O1	O2⋯H4	C5⋯O2	O1⋯H4
ts-i45	1.16	0.24	0.41	0.55
	N2⋯C5	O1⋯H4	H4⋯N2	C5⋯O1
ts-i56	0.38	0.73	0.12	1.26
	N2⋯C4	N2⋯H4	H4⋯O3	C4⋯O3

ts-V3a	0.65	0.44	0.31	1.24
	N1⋯Rh	Cl4⋯H5	H5⋯N1	Rh⋯Cl4
ts-i78	0.37	0.44	0.47	0.13
	C6⋯C7	C6⋯O3	C7⋯H6	H6⋯O3
ts-3bin1	0.33	0.45	0.27	0.44
	C8⋯H7	H7⋯C10		
ts-Ain2	0.12	0.69		
	C10⋯H7	H7⋯C1		
ts-in23	0.64	0.16		
	C1⋯H7	H7⋯O4	C4⋯O4	
ts-in34	0.45	0.36	0.44	

Figure S1. Evolution of bond lengths along the IRC for (a) **ts-i12** (b) **ts-IIIII** (c) **ts-i3IV** (d) **ts-i45** (e) **ts-i56** (f) **ts-V3a** (g) **ts-3bin1** (h) **ts-Ain2** (i) **ts-in23** (j) **ts-in34** at B3LYP/6-311++G(d,p) level.

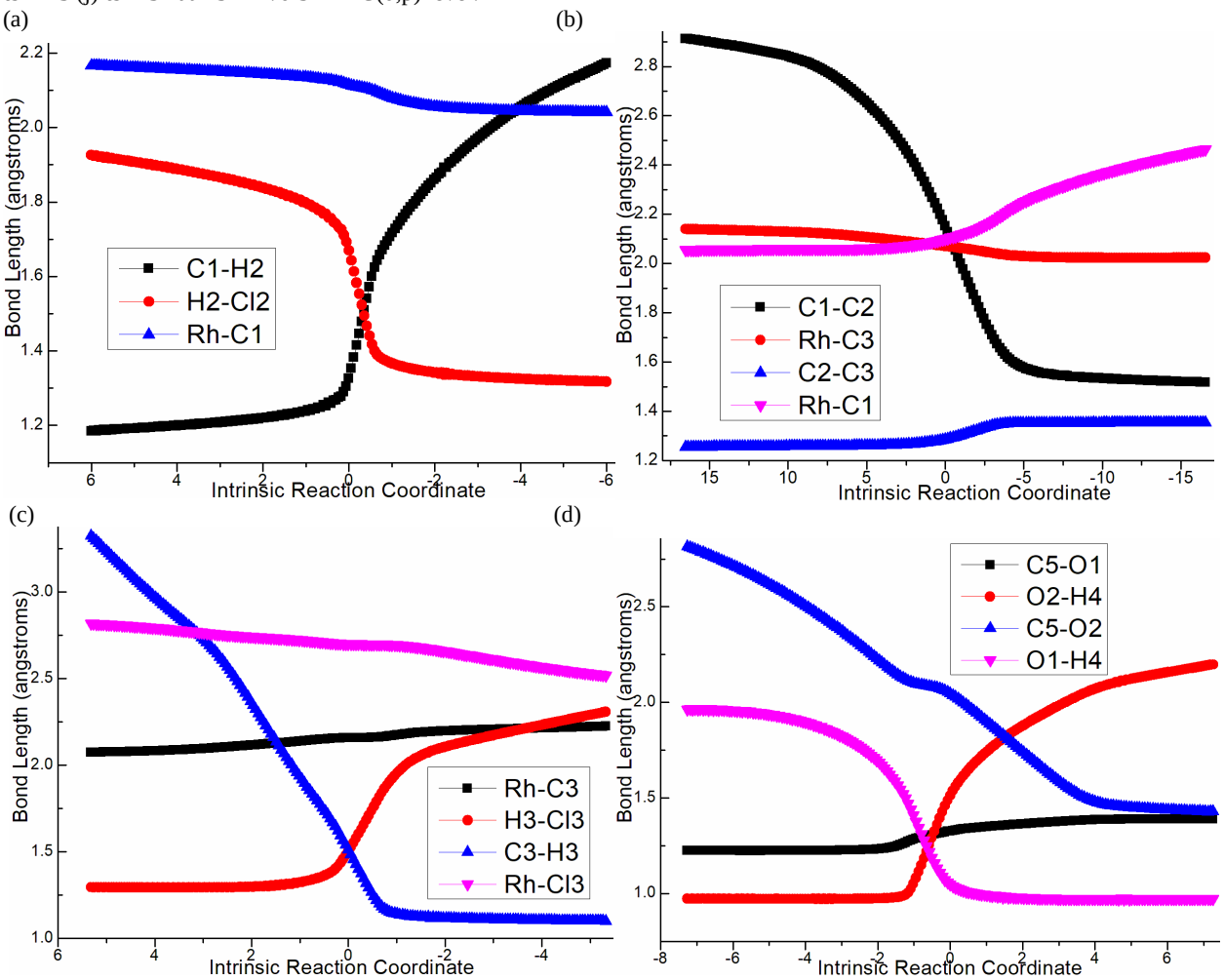

(e)

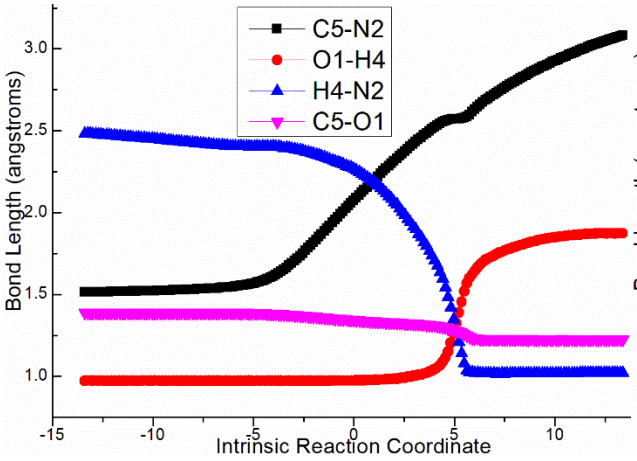
C5-N2
O1-H4
H4-N2
C5-O1
Bond Length (angstroms)
Intrinsic Reaction Coordinate

(f)

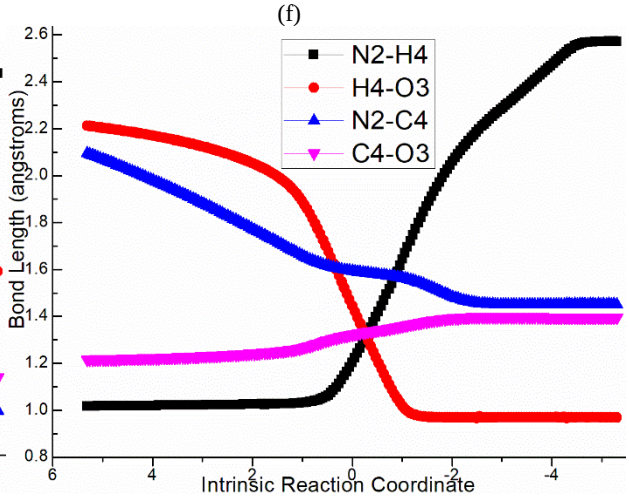
N2-H4
H4-O3
N2-C4
C4-O3
Bond Length (angstroms)
Intrinsic Reaction Coordinate

(g)

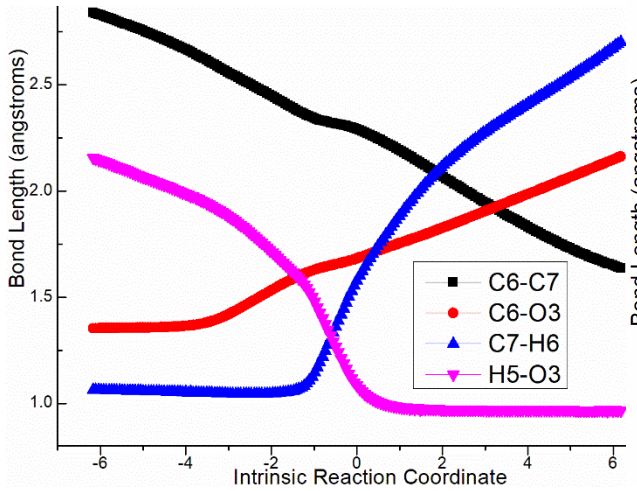
C6-C7
C6-O3
C7-H6
H5-O3
Bond Length (angstroms)
Intrinsic Reaction Coordinate

(h)

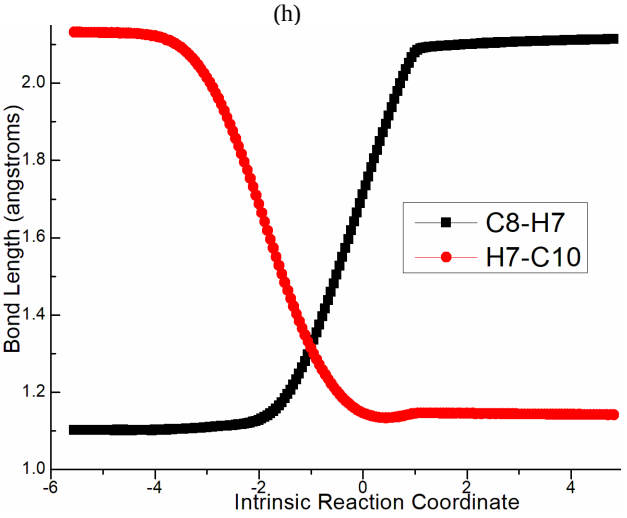
C8-H7
H7-C10
Bond Length (angstroms)
Intrinsic Reaction Coordinate

(i)

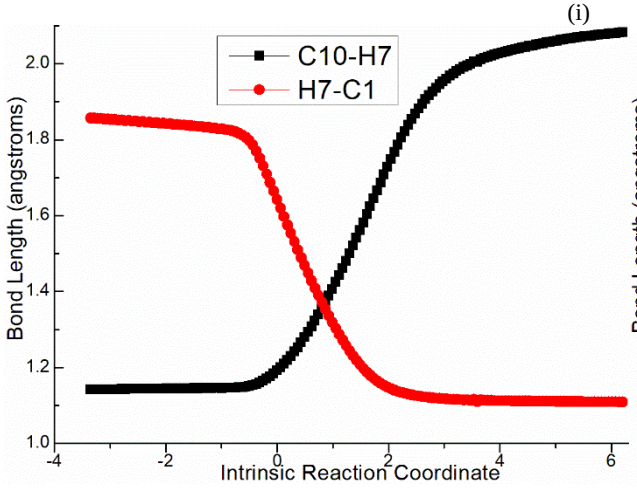
C10-H7
H7-C1
Bond Length (angstroms)
Intrinsic Reaction Coordinate

(j)

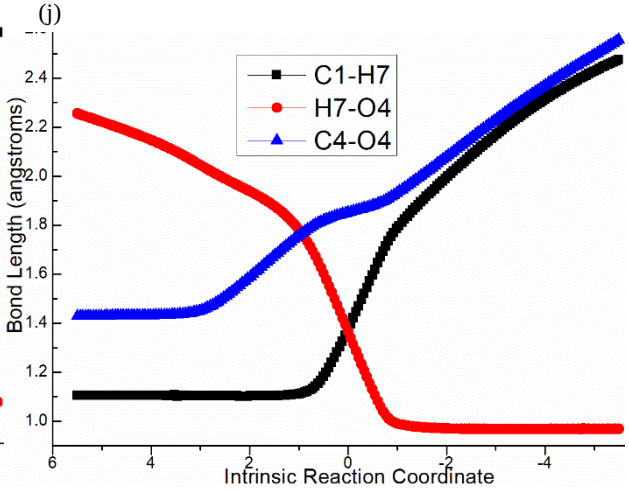
C1-H7
H7-O4
C4-O4
Bond Length (angstroms)
Intrinsic Reaction Coordinate

Figure S2. Highest Occupied Molecular Orbital (HOMO) of typical TSs. Different colors are used to identify the phase of the wave functions.

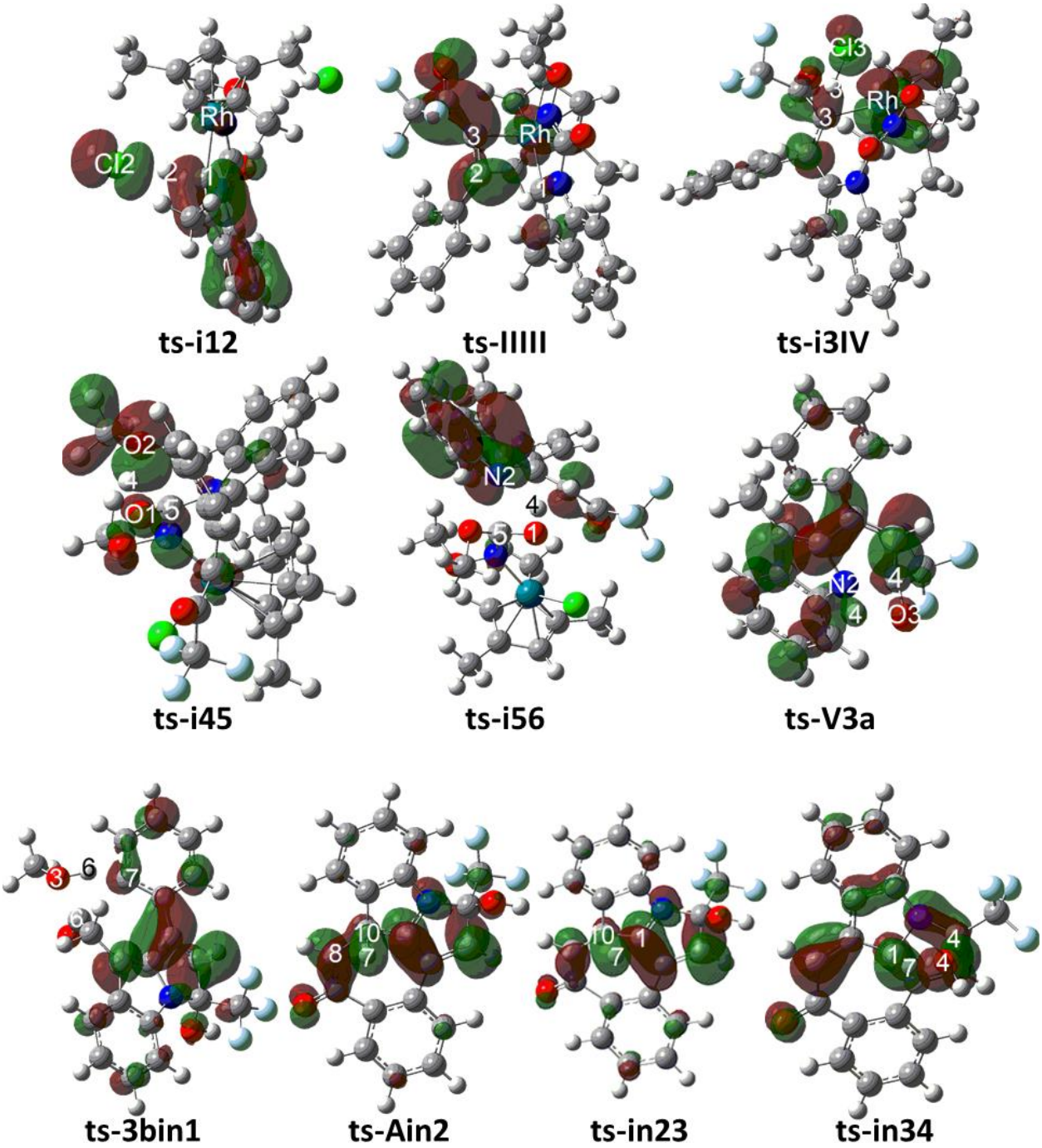

DOI:10.31579/2690-1897/198